

Cutaneous Ionogel Mechanoreceptors for Soft Machines, Physiological Sensing, and Amputee Prostheses

Zequn Shen, Xiangyang Zhu, Carmel Majidi,* and Guoying Gu*

Touch sensing has a central role in robotic grasping and emerging human-machine interfaces for robot-assisted prosthetics. Although advancements in soft conductive polymers have promoted the creation of diverse pressure sensors, these sensors are difficult to be employed as touch skins for robotics and prostheses due to their limited sensitivity, narrow pressure range, and complex structure and fabrication process. Here, a highly sensitive and robust soft touch skin is presented with ultracapacitive sensing that combines ionic hydrogels with commercially available conductive fabrics. Prototypical designs of the capacitive sensors through facile manufacturing methods are introduced and a high sensitivity up to 1.5 kPa^{-1} (≈ 44 times higher than conventional parallel-plate capacitive counterparts), a broad pressure detection range of over four orders of magnitudes ($\approx 35 \text{ Pa}$ to 330 kPa), ultrahigh baseline of capacitance, fast response time ($\approx 18 \text{ ms}$), and good repeatability are demonstrated. Ionogel skins composed of an array of cutaneous mechanoreceptors capable of monitoring various physiological signals and shape detection are further developed. The touch skin can be integrated within a soft bionic hand and provide an industrial robot and an amputee with robust tactile feedback when handling delicate objects, illustrating its potential applications in next-generation human-in-the-loop robotic systems with tactile sensing.

1. Introduction

Designing touch-sensitive skins to mimic various functions and properties of natural epidermal tissue is an essential but open challenge in the fields of wearable electronics^[1–6] and robotics.^[7–12] Over the past decades, a number of artificial skins have been developed based on various materials—from rigid

to soft electronic components^[13,14]—and mechanisms, such as capacitive,^[3,15,16] piezoresistive,^[17,18] piezoelectric,^[19,20] triboelectric^[21,22] pressure sensors. However, these sensing architectures can be susceptible to external interference and have the potential to suffer from undesirable sensing performance in unstructured and dynamic environments when integrated with robotic systems. Recently, some studies have presented methods to improve the sensitivity or detectable limit of pressure sensors,^[3,23–29] although demonstrated integration in robotic systems for dexterous manipulation is not yet commonplace.^[16] For instance, a recent study^[30] reported an iontronic pressure sensor that uses an “intrafillable” microstructure for high sensitivity. However, despite these advancements, their reported skins are subject to either a narrow pressure detection range^[31] or a complex fabrication process for creating the microstructure^[30] that can be difficult to scale for high volume manufacturing. In addition, conventional pressure sensor designs that are more compatible for mass

manufacturing such as parallel-plate capacitive sensors^[3,16] typically exhibit low signal baseline and thus induce low signal-to-noise ratio (SNR) due to their sensitivity to environmental noise. As a result, developing robotic touch skins that provide real-time and robust tactile feedback remains a critical challenge for future intelligent robotic systems, such as soft robot grippers and prosthetic hands.

Here, we present a highly sensitive, soft iontronic touch skin with an ultrawide pressure range and resistance to external interference during robotic applications (**Figure 1a** and **Table 1**). We leverage the ultrahigh capacitance (generally on the orders of nF– μF) of the skin in order to engineer a cutaneous sensing skin that is hierarchical and size scalable. The skin is composed of ionic hydrogels and commercially available conductive fabrics that are patterned to create iontronic mechanoreceptors. This hydrogel-based architecture harnesses ultrahigh unit area capacitance ($\approx 2.14 \mu\text{F cm}^{-2}$) to achieve enhanced pressure sensing functionality with high bandwidth and sensitivity. These mechanoreceptors exhibit a high sensitivity of 1.5 kPa^{-1} , which is around $44 \times$ higher than that of their conventional parallel-plate capacitive counterparts and a broad detection range ($\approx 35 \text{ Pa}$ – 330 kPa). This class of sensors exhibits a high pressure resolution ($\approx 0.91\%$) over 113 kPa , an 18 ms response

Z. Shen, Prof. X. Zhu, Prof. G. Gu
Robotics Institute
School of Mechanical Engineering
State Key Laboratory of Mechanical System and Vibration
Shanghai Jiao Tong University
Shanghai 200240, China
E-mail: guguoying@sjtu.edu.cn
Prof. C. Majidi
Soft Machines Lab
Carnegie Mellon University
Pittsburgh, PA 15213, USA
E-mail: cmajidi@andrew.cmu.edu

 The ORCID identification number(s) for the author(s) of this article can be found under <https://doi.org/10.1002/adma.202102069>.

DOI: 10.1002/adma.202102069

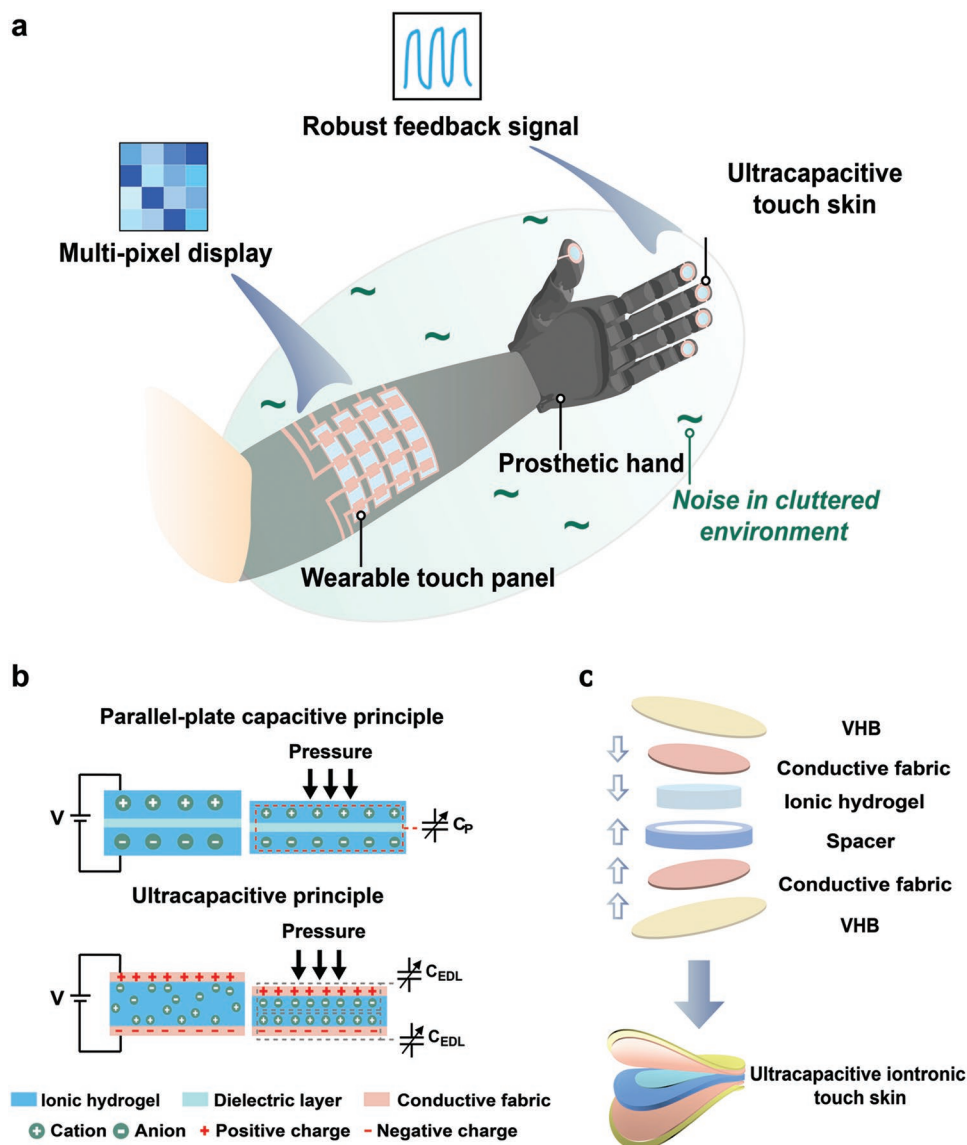


Figure 1. Design and principle of the ultracapacitive pressure-sensing robotic skin. a) Schematic illustration for the functioning of the soft robotic skin system. b) Sensing principles of the conventional parallel-plate capacitive sensor (top) and ultracapacitive sensor (bottom). For the ultracapacitive principle, the contact area between the hydrogel layer and the conductive fabric layer is limited when no pressure is applied. Positive and negative charges on the electrode layers attract relatively few cations and anions in the ionic-hydrogel layer. Under external pressure, the contact area between the layers significantly increases. More ions are attracted to the interface, thereby dramatically increasing the capacitance. c) Design architecture of the ultracapacitive iontronic pressure-sensing skin composed of ionic hydrogel, conductive fabrics, VHB elastomers and spacer.

time, which is faster than that of human skin (≈ 40 ms), and mechanical stability during 1500 compression/release cycles at a pressure of 177 kPa.

Given the high SNR and low signal crosstalk of the iontronic sensors, we demonstrate the ability to use the wearable pressure-sensing skin for continuous monitoring of various physiological signals. This includes human carotid artery pulse and detection of deep breath and cough. Moreover, we show that the skin can be utilized for a multipixel display, object shape recognition, and tactile sensing for playing a digital piano. Lastly, the iontronic touch skin introduced here is integrated within a soft bionic hand and capable of providing an industrial robot and

an amputee with real-time tactile feedback when manipulating fragile objects. Different from the existing works, the sensing functionality of our developed touch skin is achieved through intrinsic properties of the materials and does not rely on complex microstructures that may be difficult or expensive to mass manufacture. The touch skin achieves remarkable performances and enables robust robotic applications through the use of readily available materials, simple design architecture, and facile fabrication steps that are appropriate for scaled manufacturing. The application of our skin in robotic systems operating in practical environments demonstrates its promising potential for next-generation human-machine interactions and soft robotic systems.

Table 1. Comparison of the ultracapacitive iontronic pressure-sensing skins in this work with previously reported soft pressure sensors.

Ref.	Sensitivity	LOD	Limit of high pressure	Response time	Applications of robotic skins
[15]	0.01 kPa ⁻¹ (<40 kPa)	N/A	40 kPa	N/A	No
[17]	56.0–133.1 kPa ⁻¹ (< 0.03 kPa)	0.8 Pa	100 kPa	50 ms	No
[28]	0.21 kPa ⁻¹ (<2 kPa) 0.064 kPa ⁻¹ (2–10 kPa)	N/A	3.9 MPa	40 ms	No
[31]	114 nF kPa ⁻¹ (<1.33 kPa) 14.8 nF kPa ⁻¹ (1.33–10.67 kPa)	N/A	10.67 kPa	4.2 ms	No
[21]	0.013 kPa ⁻¹ (<70 kPa)	1.3 kPa	70 kPa	N/A	No
[16]	0.19 kPa ⁻¹ (<1 kPa) 0.1 kPa ⁻¹ (1–10 kPa) 0.04 kPa ⁻¹ (10–20 kPa)	0.5 kPa	100 kPa	30 ms	Yes
[45]	4.4 kPa ⁻¹ (<8 kPa)	0.3 Pa	180 kPa	N/A	Yes
[29]	48.1–33.18 kPa ⁻¹ (<5 kPa) 5.77–7.16 kPa ⁻¹ (80–135 kPa)	N/A	135 kPa	60 ms	No
[46]	1.04 V kPa ⁻¹ (<5 kPa) 0.16 V kPa ⁻¹ (5–10 kPa) 0.0014 kPa ⁻¹ (10–20 kPa) 0.0005 kPa ⁻¹ (20–120 kPa)	10 Pa	120 kPa	140 ms	Yes
[30]	3302.9 kPa ⁻¹ (<10 kPa) 671.7 kPa ⁻¹ (10–100 kPa) 229.9 kPa ⁻¹ (100–360 kPa)	0.08 Pa	360 kPa	9 ms	No
[26]	3.88 V kPa ⁻¹ (0.1–4.3 kPa) 0.54 V kPa ⁻¹ (4.3–9.8 kPa)	0.1 kPa	9.8 kPa	N/A	No
[27]	21 kPa ⁻¹ (<0.1 kPa) 0.016 kPa ⁻¹ (0.1–1 kPa)	N/A	1 kPa	90 ms	No
[3]	0.141 kPa ⁻¹ (<1 kPa) 0.010 kPa ⁻¹ (10–100 kPa)	N/A	100 kPa	190 ms	No
[44]	15.22 kPa ⁻¹ (<5 kPa) 0.51 kPa ⁻¹ (5–45 kPa)	100 Pa	45 kPa	74 ms	No
[43]	5.49 kPa ⁻¹ (<0.5 kPa) 0.65 kPa ⁻¹ (0.5–7 kPa) 0.01 kPa ⁻¹ (7–460 kPa)	N/A	460 kPa	75 ms	No
This work	0.24 kPa ⁻¹ (<70 kPa) 1.5 kPa ⁻¹ (70–150 kPa) 0.13 kPa ⁻¹ (150–330 kPa)	35 Pa	330 kPa	18 ms	Yes

2. Results and Discussion

2.1. Sensing Principle and Design of the Ionogel Pressure Sensor

The ultracapacitive ionogel pressure sensor is composed of an ionic-hydrogel solid electrolyte layer that is covered on both sides with metal-plated conductive fabric electrodes. Hydrogels feature high porosity that facilitates the increase of contact area between hydrogels and flexible fabric electrodes under compression.^[32] In this way, the iontronic sensor differs from more conventional designs for parallel-plate capacitive sensing (Figure 1b).^[33] We choose polyacrylamide (PAAm) hydrogels containing NaCl as the ionic conductor owing to their facile fabrication process, excellent mechanical properties, biocompatibility, and ionic conductivity.^[15] The hydrogel is surrounded by a spacer ring made of silicone rubber (Ecoflex 00-30, Smooth-On) with a higher elastic modulus than that of ionic hydrogels. This elastomer spacer can function as a supporting frame, allowing

for the fast recovery of the elastic hydrogel after the removal of external pressure and alleviating the adverse influence of viscoelastic hysteresis. In addition, to prevent the dehydration of ionic hydrogels and ensure robust sensing properties, we utilize two polyacrylate elastomers (VHB 4905, 3M Very High Bond tape) to encapsulate the total structure. These materials are selected on account of their commercial availability and mechanical stability. These components are assembled by means of lamination, resulting in the hierarchical structure shown in Figure 1c. The fabrication and assembly process of the sensors can be scaled readily and is not limited to specific dimensional configurations.

Different from the conventional capacitive pressure-sensing principle (see the Supporting Information), the iontronic capacitor substitutes the intermediate dielectric layer with an ionically conductive hydrogel. This iontronic structure generates the interfacial capacitance that is referred to as the electric double layer (EDL) capacitance.^[34] There are mobile cations and anions in ionic hydrogels, while a sufficient number of

free electrons exist on the surface of the metal-plated fabric layers. When voltage is applied, positive and negative charges on two electrode layers attract ions with opposite polarity in the ionic-hydrogel layer, respectively. Numerous electron–ion pairs constitute microscale capacitors with nanometer separation distance and thus induce ultrahigh capacitance per unit area, which is up to around 10^3 times more than that of parallel-plate capacitors.^[35] When the external pressure is exerted, the contact area between the ionic-hydrogel layer and the conductive fabric layers significantly increases due to the intrinsic microstructures of the conductive fabrics. We inspect the microscopic morphological features of the commercially available conductive fabric electrode using scanning electron microscopy and atomic force microscopy (AFM). The experimental results (Figure S1, Supporting Information) demonstrate that there are dense, uneven microstructures on the surface of the metal-plated conductive fabric, which will contribute to the significant rise of the contact area between layers under the applied pressure.^[17,30] More electron–ion pairs are aggregated and relocated at interfaces, inducing a dramatic increase of the capacitance. The strong interfacial capacitive coupling established by mobile ions and electrons exhibits enhanced stimuli-responsive behavior that results in highly sensitive and robust pressure sensing.

2.2. Sensing Properties of the Ionogel Pressure Sensor

We fabricate this class of ultracapacitive ionogel pressure sensors (more details on fabrication in Figure S2, Supporting Information) and characterize their sensing properties including sensitivity, detection range, response time, mechanical durability, and high-pressure resolution. Pressure sensitivity S is a key criterion revealing the sensitive ability of sensors, which is generally defined as $S = \delta(\Delta C/C_0)/\delta P$, where ΔC is the change of capacitance, C_0 is the initial capacitance without exerted pressure, and P is the applied pressure. Compared with the classical parallel-plate capacitive sensor, our developed ultracapacitive ionogel pressure sensor exhibits the similar sandwiched structure but different sensing principle. To demonstrate the improvement of our iontronic sensing principle, we fabricate both types of sensors using the same commercial materials. The parallel-plate capacitive sensors are fabricated with the same dimensions using 3M VHB elastomer as the dielectric material (see Figure S3, Supporting Information), similar to other previous work on soft capacitive sensors.^[36] As shown in Figure 2a, the ultracapacitive iontronic sensor exhibits a high sensitivity of 0.24 kPa^{-1} when the pressure is below 70 kPa, 1.5 kPa^{-1} within the pressure range of 70–150 kPa, and 0.13 kPa^{-1} in the high pressure regime of 150–330 kPa. In contrast, the maximum sensitivity of the conventional capacitive sensor is found to be 0.034 kPa^{-1} . Under the equivalent applied pressure, the relative change of capacitance of ultracapacitive iontronic sensor is more significant and thus its maximum sensitivity is around $44 \times$ higher than that of its conventional dielectric elastomer counterpart. Moreover, due to the formation of the EDL, the values of initial and maximum capacitance of iontronic sensors are up to approximately three to five orders of magnitude higher than that of the parallel-plate

capacitive sensors. As shown in Figure 2b,c, iontronic sensors exhibit an ultrahigh initial capacitance $C_0 = 5.65 \text{ nF}$ and maximum capacitance $C_{\text{max}} = 605 \text{ nF}$. For comparison, the parallel-plate capacitive sensors have an initial capacitance $C_0 = 0.0023 \text{ nF}$ and maximum capacitance $C_{\text{max}} = 0.0211 \text{ nF}$. Since the parasitic and environmental noise is generally on the order of pF,^[31] the dramatic elevation of capacitance allows sensors to avoid interference of capacitive noise within the internal circuits and external environment, contributing to robust measurement in practical applications. We further explore several key factors influencing the sensitivity of ionogel pressure sensors. First, frequency dependence is a typical feature of capacitive devices that utilize the EDL phenomena, where the capacitance value decreases with the increase of test frequency (Figure S4, Supporting Information).^[29] The test frequency refers to the frequency of the test signal (AC) in the capacitance measurement circuit. Under different test frequency conditions, the range of relative change in capacitance signals is different, which influences the characterization of the sensitivity of iontronic pressure sensors. As shown in Figure S5 in the Supporting Information, high frequencies such as 100 kHz are demonstrated to allow for the characterization of higher sensitivity. Additionally, the effective sensing area and thickness of the pressure sensor also influence sensitivity and/or detection range. Figure S6 in the Supporting Information presents the capacitance response of ultracapacitive sensors with different dimensions, for example, sensors with thicker ionic-hydrogel layers exhibit higher sensitivity. However, too much thickness will cause the sensor to be uncomfortable on human skin and can contribute to a loss of natural sensation when incorporated into a wearable device.^[3] To address this, the geometric dimensions of the iontronic material can be configured according to specific requirements of fabrication and application in order to tailor the sensor's sensitivity. Notably, the voltage across the soft sensors under test is controlled within the potential window to avoid the adverse effect of interfacial electrochemical reactions (see Figures S7 and S8, Supporting Information).^[15]

Next, we evaluate other critical electrical and mechanical properties of our ionogel pressure sensors. The maximum detectable pressure reaches up to 330 kPa (Figure 2a), much higher than the typical sensitive range of human skin ($\approx 10 \text{ kPa}$).^[16] Meanwhile, the sensor exhibits a limit of detection (LOD) of 35 Pa, representing the ultimate detection capability for ultralow pressure (Figure 2d). To evaluate this property, a weight of 100 mg is gently placed on our pressure sensor and then quickly removed. Despite the capacitive fluctuation under the LOD pressure, the signal quality is sufficient to accurately detect the touch of an ultralow pressure. This process also reveals a pressure-response time of 18 ms and a release time of 36 ms, faster than the responsive speed of human skin ($\approx 40 \text{ ms}$).^[37] Notably, due to the internal ionic motions, the response time of the iontronic pressure sensor will increase with a higher applied pressure (Figure S9, Supporting Information). When the sensor is under periodic loads within different pressure regimes such as 42, 85, and 162 kPa, it presents reliable pressure-responsive capability (Figure 2e). Furthermore, its electrical property exhibits no obvious attenuation ($< 2.3\%$) after over 1500 loading/unloading cycles at an ultrahigh pressure of 177 kPa (Figure 2f). In the low pressure regime

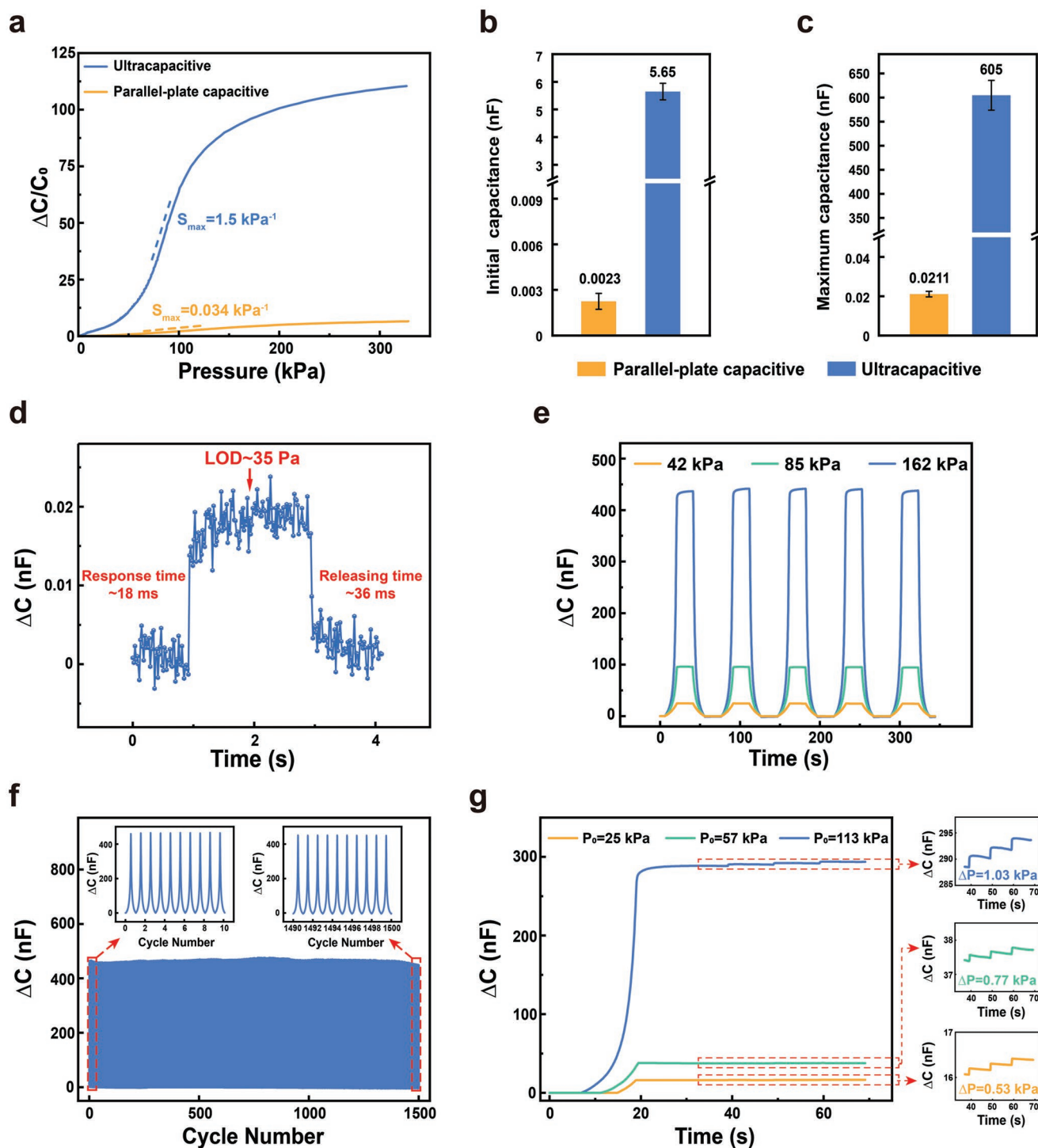


Figure 2. Characterization of the ultracapacitive iontronic pressure sensor. a) Comparison of pressure sensitivities of the ultracapacitive pressure sensor and the parallel-plate capacitive sensor. b,c) Comparison of initial capacitance (under no external pressure) and maximum capacitance (under the pressure of 330 kPa) between the ultracapacitive sensor and the parallel-plate capacitive sensor. d) Instant response of the pressure sensor, which exhibits limit of detection (LOD) of 35 Pa, a response time of 18 ms, and a releasing time of 36 ms. e) Capacitance response of the ultracapacitive pressure sensor under periodic loading pressures of 42, 85, and 162 kPa, respectively. f) Cycling stability at a high pressure of 177 kPa (1500 cycles). The insets show the first ten cycles and the last ten cycles. g) Detection of sequential subtle pressures with three initial loading pressure levels (25, 57, and 113 kPa).

(≈ 20 kPa), the sensor maintains robustness during 5000 cycles (Figure S10, Supporting Information). The electromechanical durability under the long-term cyclic loading condition is a

crucial factor influencing the robust applications of our pressure sensors. These characterizations of sensing performance also demonstrate that our sensor exhibits fast recovery when

load is removed. In addition, the resolution in the high-pressure regime of a pressure sensor determines its detection capability for subtle changes in pressure after an initial pressure P_0 has already been applied. As shown in Figure 2g, when P_0 of 25, 57, and 113 kPa have been loaded, our pressure sensor exhibits a high pressure resolution of 0.53 kPa (2.12%), 0.77 kPa (1.35%), and 1.03 kPa (0.91%), respectively. The aforementioned desirable sensing properties indicate that our ultracapacitive iontronic pressure sensor is a promising candidate for practical applications of wearable skins and prosthetic robots that rely on both high bandwidth and sensitivity.

2.3. Wearable Pressure-Sensing Electronic Skins

In natural human skin, different types of mechanoreceptors^[38] are responsible for sensing under various pressure loading regimes. For example, Merkel cells and Meissner's corpuscles are utilized for light-touch stimulus, while Pacinian corpuscles rapidly detect gross contact and deep pressure in the skin.^[39,40] The pressure detection range of our electronic skin can cover that of various mechanoreceptors in natural skin. As depicted in Figure 3a, the touch skin is capable of accurately

distinguishing continuous gentle touch (≈ 40 kPa), medium touch (≈ 90 kPa), and heavy touch (≈ 120 kPa) with fast response akin to human skin. To further explore its instantaneous response capability in practical applications, we measure the change of capacitance signal as water drops fall onto the surface of electronic skins (Figure 3b). The acquired capacitance exhibits dramatic change at the moment when a water drop (weight of about 380 mg) falls from different heights, and the higher dropping height results in a greater change of capacitance. Referring to the figure, we observe that the capacitance signal rises and immediately falls back to the initial value within 46 ms, indicating that our ultrasensitive iongel mechanoreceptors can mimic human skin in response to instantaneous external stimuli. Based on the above-mentioned high sensitivity and flexibility, we demonstrate the ultracapacitive iontronic skins as a wearable pressure-sensing device for healthcare monitoring and clinical diagnosis. The electronic skin is attached to a healthy subject's neck and applied to detect carotid artery pulse waveforms and heart rate ($100 \text{ beats min}^{-1}$) (Figure 3c). As shown in the inset, the recorded capacitance signal presents typical characteristics of normal carotid artery pulse waveforms, including "P" (percussion), "T" (tidal), and "D" (diastolic).^[41] The detection result can be utilized to

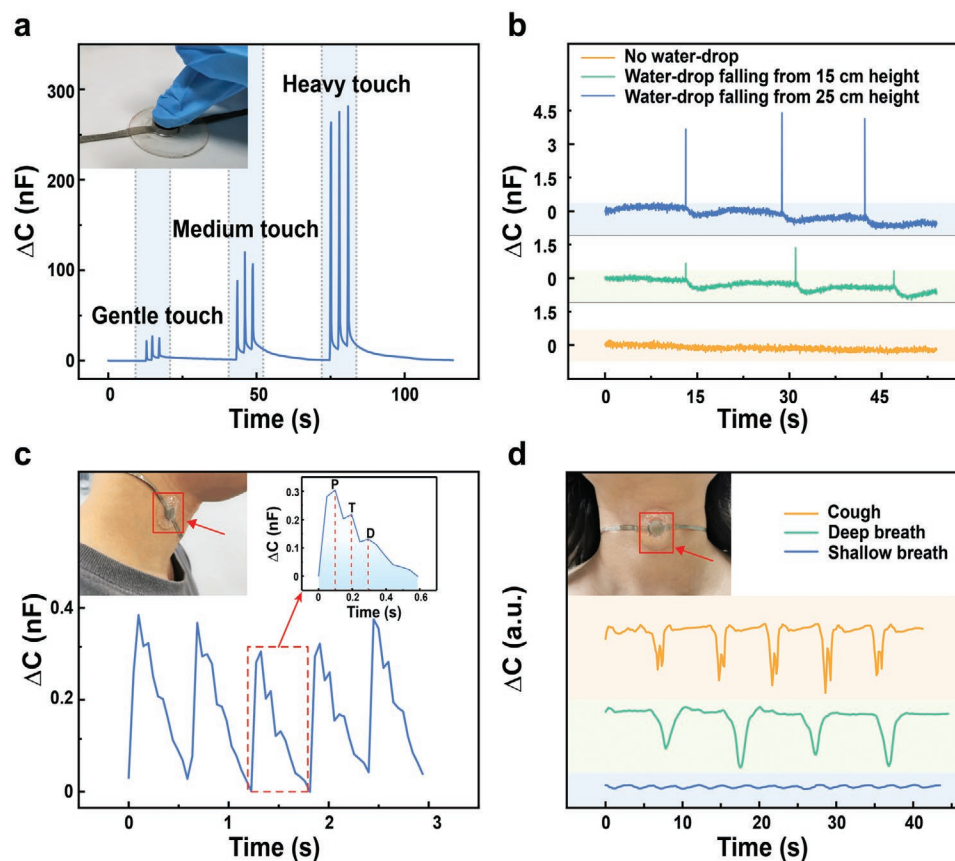


Figure 3. Wearable iongel mechanoreceptors for physiological signal monitors. a) The change in capacitance signals when compressed by human fingers with different pressures, i.e., gentle touch (≈ 40 kPa), medium touch (≈ 90 kPa) and heavy touch (≈ 120 kPa). The inset shows a photograph of a sensor sample pressed by a finger. b) Real-time measurement in response to the water droplets (380 mg) continuously falling from different heights. c) Real-time monitoring of human carotid artery pulse. The left inset shows that the electronic skin is attached to skin near the right carotid artery. The right inset demonstrates the typical features of carotid artery pulse waveforms. d) Real-time monitoring of human shallow breath, deep breath, and cough, respectively. The inset shows the electronic skin attached to the throat.

medically access heart health and diagnose vascular aging. In addition, the touch skin is capable of monitoring and distinguishing other types of physiological signals such as shallow breath, deep breath, and cough in real time (Figure 3d). The robust electronic skin is insensitive to electrical interferences in practical environments such as body movements. As shown in Figure S11 in the Supporting Information, the electronic skin attached to the subject's chest can continuously monitor breathing while the subject is running in place and standing still, respectively. In contrast to current rigid and cumbersome medical instruments, our soft flexible electronic skins provide a low-cost, noninvasive, and convenient method for biosensing in practical biomedical applications.

2.4. Multipixel Sensing Arrays

We present wearable multipixel sensing arrays based on the ultracapacitive ionogel mechanoreceptors in order to demonstrate the ability to perform sensing with multiple nodes. Due to the high capacitance value, our iontronic pressure sensors are not susceptible to external noise interference, compared to the conventional parallel-plate capacitive pressure sensors. When expanded to a multiplex sensing array, the adverse signal crosstalk and biased measurement will be effectively avoided. We compare the SNR of ultracapacitive ionogel sensors and parallel-plate capacitive sensors at a low pressure (≈ 20 kPa) and a high pressure (≈ 177 kPa), respectively. As shown in Figure S12 in the Supporting Information, the SNR of iontronic pressure sensors reach up to 61.41 and 88.51 dB at the corresponding testing conditions, significantly higher than that of their counterparts. Further, an iontronic skin-attached piano strip is accordingly designed (Figure 4a). The sensing structure is encapsulated in 3M VHB tape, which allows for adhesion to human skin without the need for additional bonding layers. The 1D touch strip enables seven channels of pressure detection and plays different musical notes (i.e., do, re, mi, fa, sol, la, ti) corresponding to the acquired capacitive signals. Figure 4b shows that the relative change of capacitance of the touched channel is distinctly large ($\Delta C/C_0 > 0.3$) compared to the relatively small fluctuations of other untouched channels caused by the negligible signal crosstalk. In Movie S1 in the Supporting Information, this interactive piano strip is shown to be conformal with human skin and can be used to play a continuous melody in real-time when various channels are successively touched, indicating its fast, multiplexed pressure-responsive capability. The wearable touch strip can provide stable signals and sensing functions for long-term monitoring of more than 90 min (Figure S13, Supporting Information).

Additionally, a 2D touch panel employing the iontronic principle is explored. We design a calculator with a 4×4 array of buttons based on the similar hierarchical structure (Figure 4c). The 2D sensing panel consists of four strips of ionic hydrogel and an orthogonal 4×4 electrode array. The pressure causes a dramatic increase of capacitance of the touched pixel, while the surrounding untouched pixels exhibit only slight change in capacitance (Figure 4d). This 2D touch panel is thus capable of accurately detecting the position of contacted pixels and transforming the position to a control signal for performing

calculations and displaying results (see Movie S2, Supporting Information).

To demonstrate the simultaneous detection capability of the multipoint touch panel, we also develop a sensing array enabling 2D-shape recognition (Figure 4e). The pressed area can be distinguished from the unpressed area through the synchronous capacitance response of pertinent pixels without obvious mutual interferences and time delay (Figure 4f). In Movie S3 in the Supporting Information, when the blocks are placed on the sensing array in a random order, the shape of blocks can be accurately recognized and displayed via a light-emitting diode (LED) nixie tube.

2.5. Robotic Skins for Prostheses with Tactile Feedback

Tactile sensation and feedback play a key role in the grasping and manipulation of human hands. However, most of existing pressure sensors are difficult to be used in a prosthetic skin due to the noise interference that arises in practical applications. Our previously reported soft bionic hand^[42] employs conventional parallel-plate capacitive pressure sensors, which provide limited tactile sensing capability. Here, we demonstrate the ability to overcome these past limitations with a soft bionic hand that is integrated with our ultracapacitive iontronic touch skins, which allows for high dexterity and enhanced versatility. As shown in Movie S4 in the Supporting Information, the flexible touch skins are conformally mounted on the five fingertips and will not interfere with free deformations of the soft pneumatic bionic hand. Some small objects such as a nut (weight, 340 mg) are gently placed on the fingertips of the bionic hand, and the multichannel capacitance signals are recorded in real time (Figure 5a). Further, when a feather (weight, 320 mg) is placed on the fingertip of the ring finger, the corresponding sensing channel also presents a measurable increase of the capacitance signal (Figure 5b). In addition to the capability of detecting lightweight objects, we also demonstrate that the sensory bionic hand can capture dynamic and consecutive pressure stimuli. The multichannel response results are plotted in Figure 5c when a tennis ball (weight, 58 g) successively rolls over four fingertips of the soft hand, while the untouched thumb corresponds to the pressure signal near zero. In another interactive experiment, each finger is programmed to bend as soon as its fingertip is touched and the change of capacitance is above a threshold (i.e., the threshold $\Delta C = 10$ nF) (Figure 5d). The touch-activated fingers show fast responsive movements interacting with external pressure stimuli, which indicate that our touch skins can be coordinated with robotic systems. Notably, the bending deformations of the pneumatic fingers have no significant influence on the stable capacitive signals of our robotic skin, demonstrating its mechanical robustness under bending conditions. Moreover, our touch skin possesses dynamic response capabilities required to control the movement of an industrial robot in real time. Referring to Figure 5e and Movie S5 in the Supporting Information, the sensory bionic hand is fixed on an industrial robot that is programmed to execute forward movement (0.1 m s^{-1}) unless the touch of a feather is detected. When the ultralight feather (67 mg) touches the iontronic skin, the industrial robot with

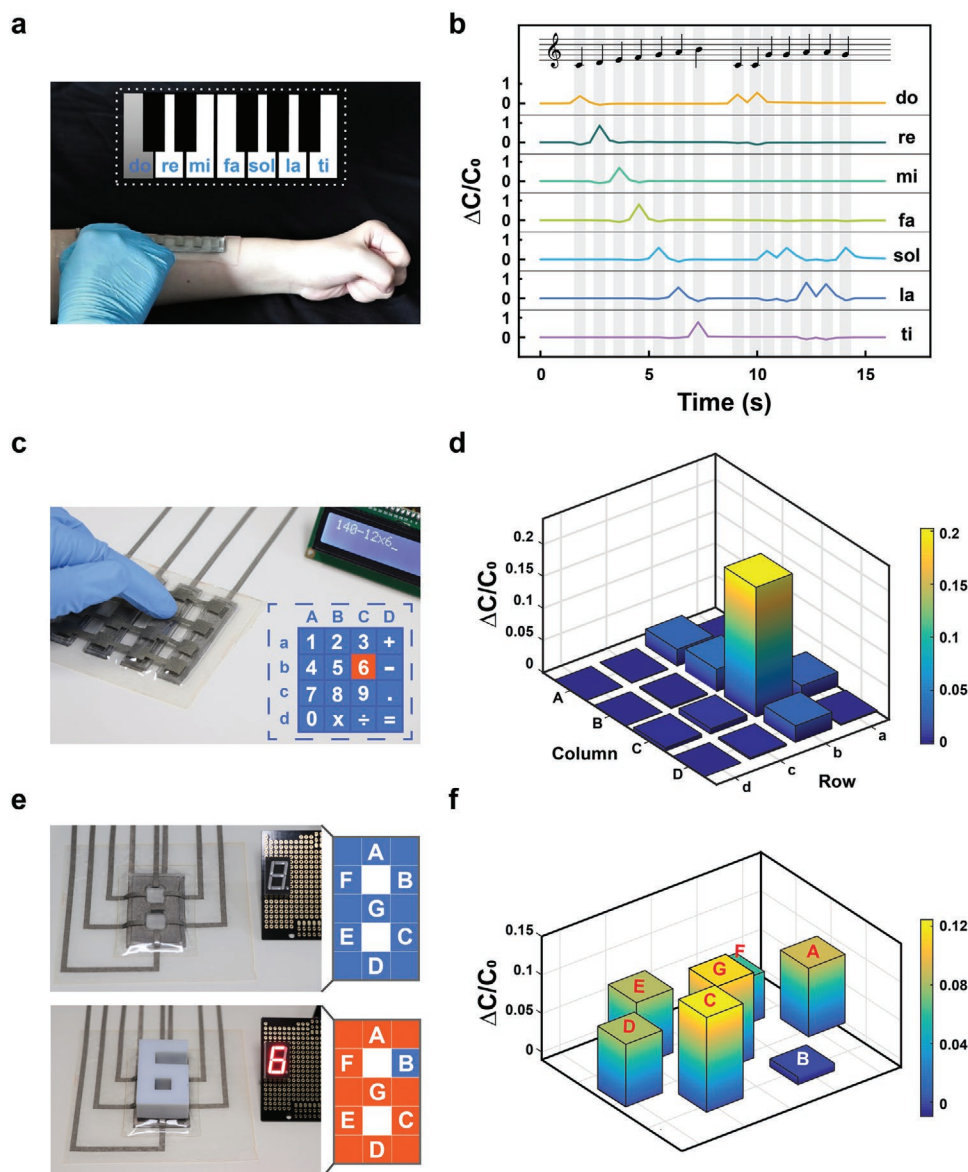


Figure 4. Applications of the multiplex sensing arrays. a) A 1D touch strip mounted on the human forearm that enables piano playing. The inset shows a schematic depiction of the seven keys of a piano. b) Relative change in capacitance ($\Delta C/C_0$) of seven channels in the touch strip during the playing of a melody. c) A 2D calculator touch panel with 4×4 pixels. The inset shows a schematic depiction of the calculator. d) Capacitance distribution mapping of 16 pixels. e) A 2D sensing array enabled to recognize the shapes of testing patterns. The inset shows a schematic depiction of the pressure-sensing pixels on the array. f) Capacitance distribution mapping of the sensing array. The height of the columns corresponds to the relative change in capacitance ($\Delta C/C_0$).

the soft bionic hand immediately interrupts the forward movement and then executes the preprogrammed backward movement. The real-time capacitance response result is plotted in Figure 5f, indicating the ultrasensitive detection capability and high SNR of our touch skin in a dynamic robotic application.

We further demonstrate a human-in-the-loop robotic system through a transradial amputee using the neuroprosthetic hand with tactile sensing. **Figure 6a** illustrates an experiment where the subject uses electromyography to control the prosthetic hand to manipulate fragile objects such as a cake. We compare the single-channel capacitance signal (index finger) of the touch skin during the manipulation with and without tactile feedback

(Figure 6b and Movie S6, Supporting Information). The prosthetic user without tactile sensing has no detailed information about the interaction and is observed to repeatedly deform the cake. By contrast, the subject using a sensory prosthetic hand can be informed by a prompt tone when the capacitance signal surpasses a threshold ($\Delta C/C_0 = 0.1$) that alerts him to stop pressing on the delicate object. Another experiment utilizes multilevel tactile feedback through three thresholds of $\Delta C/C_0$ ($T_I = 0.05$, $T_{II} = 0.1$, $T_{III} = 0.14$). The subject can sense the magnitude of output force according to three-level prompt tones in the interaction with fragile objects, which mimics the close-loop control of human grasping and manipulation (Figure 6c and

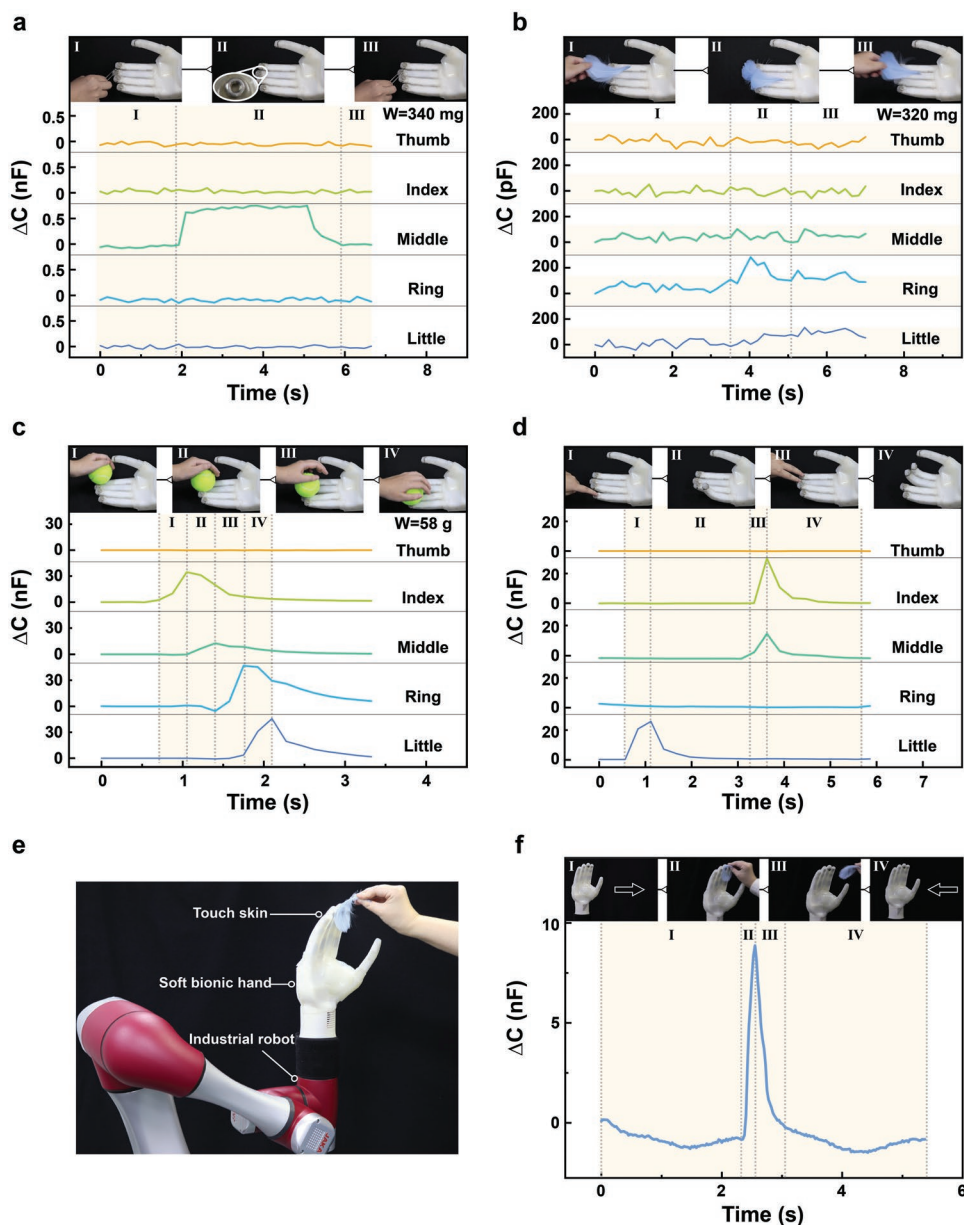


Figure 5. Ultrasensitive touch skin for a soft bionic hand. a,b) Real-time multichannel capacitance signals of the touch skin mounted on a soft bionic hand, corresponding to the loading and removal of a) a lightweight nut (weight, 340 mg) and b) a feather (weight, 320 mg). c) Multichannel capacitance signals of the robotic skin when a tennis ball (weight, 58 g) rolls over the bionic hand. d) The touched individual finger or multiple fingers are programmed to bend when the corresponding change in capacitance surpasses the threshold ($\Delta C = 10$ nF). e) Photograph of the experimental setup with the sensory bionic hand fixed on an industrial robot. The industrial robot is programmed to move forward unless the ultralight feather is detected. f) Real-time capacitance signal of the touch skin during the dynamic response process. The inset photographs show the interaction process of the sensory bionic hand.

Movie S7, Supporting Information). Additionally, we demonstrate that the ultrasensitive robotic skin enables the amputee to discriminate objects in daily life with different shapes such as a ripe tomato, a subacute carambola, and a prickly pineapple (Figure 6d). When the amputee with the sensory prosthetic hand presses different fruits with the same force, different surface shapes will induce different pressure and thus different levels of capacitive signals. Notably, the surface feature of the sponge cake is similar to the ripe tomato, both without a subacute

edge and sharp thorn. Therefore, the capacitive response of the cake is on the same order with that of the tomato.

3. Conclusion

We present a soft ultracapacitive ionic-hydrogel based tactile skin capable of providing pressure-sensing for wearable electronics and prosthetic robots. We compare our touch skin

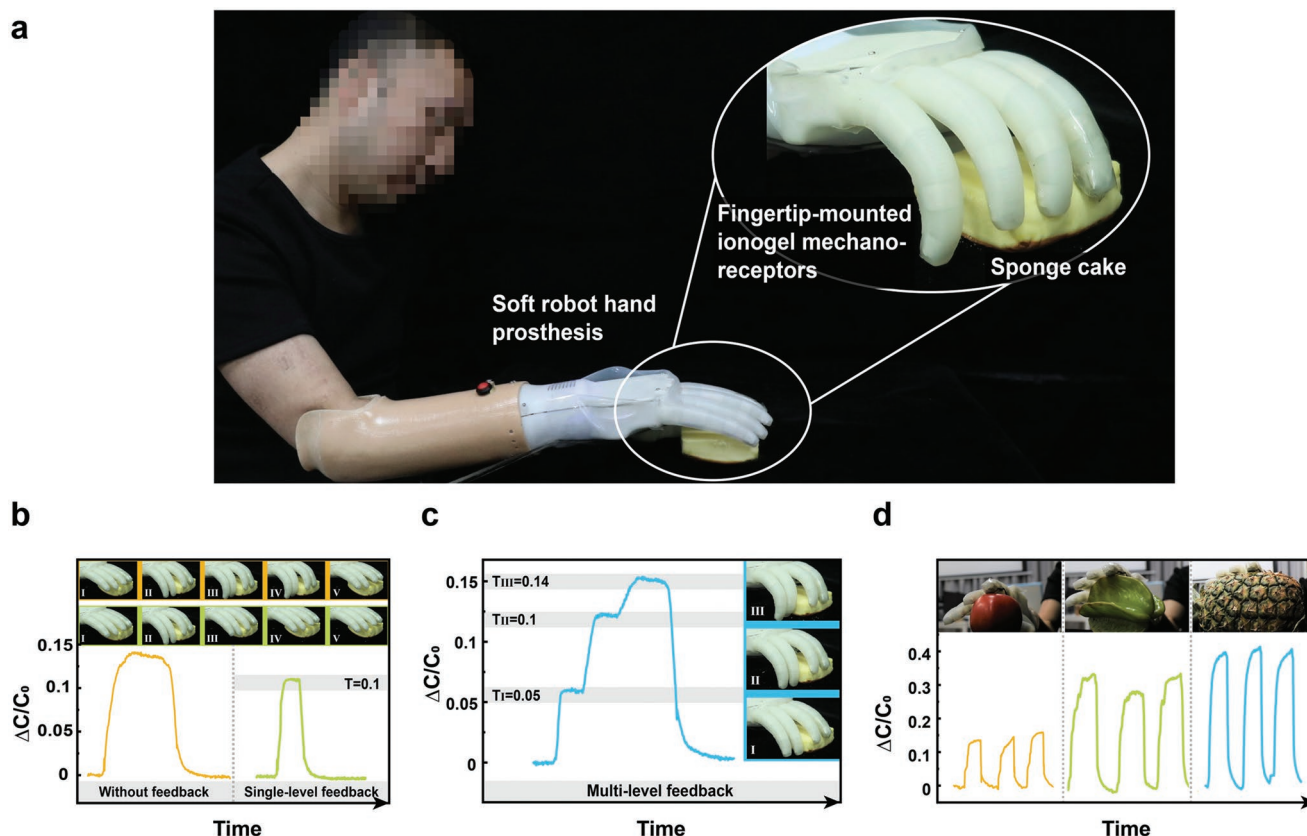


Figure 6. Human-in-the-loop robotic systems with tactile ionogel mechanoreceptors. a) Photograph of a transradial amputee using a soft prosthetic hand integrated with touch skin that interacts with fragile objects such as a cake. b) Comparison of the pressure response of the sensory prosthetic hand when manipulating a cake, without tactile feedback and with single-level feedback. The threshold of single-level feedback is $\Delta C/C_0 = 0.1$. The inset photographs show operation process of pressing. c) Multilevel tactile feedback during continuous pressing on a cake. The three-level thresholds of $\Delta C/C_0$ are 0.05, 0.1, and 0.14, respectively. The inset photographs show three stages of the pressing process. d) Demonstration of the capability of the sensory prosthetic hand to distinguish objects with different shapes (ripe tomato, subacute carambola, and prickly pineapple).

with previously reported soft pressure sensors based on hydrogels^[15,17,21,30] and other conductive soft materials.^[3,16,26–29,31,43–46] The results demonstrate that our touch skin enables robust robotic applications and achieves superior sensing performances—including high sensitivity and resolution, fast response speed, and a broad detection range (see Table 1). The robotic skin can provide an industrial robot and a transradial amputee with real-time sensory feedback, which facilitates dexterous manipulation and secure interaction with the external environment. In addition to the ionic hydrogels used here, newly developed iontronic materials can be further explored in future works. To improve the level of miniaturization and integration of robotic systems, future studies should focus on wireless acquisition and transmission equipment for ultrahigh capacitance (on the orders of nF to μ F). Accurately modeling and predicting the sensitivity of iontronic sensors also remains an open challenge,^[35] requiring the further explorations. Additionally, our touch skins have the potential to be engineering with a higher density of pixels and larger surface area, which we hope to explore in future works. Moreover, because of their versatile material architecture, the skins can potentially be integrated with more effective tactile feedback methods such as electrical and vibration stimulation. The use of the ultracapacitive

iontronic material as a novel electronic skin suggests new possibilities in the next-generation of human–machine interfaces, prosthetics, and other intelligent robotic systems.

4. Experimental Section

Preparation of Ionic Hydrogels: The PAAm-NaCl hydrogels were prepared according to the method^[47] previously reported. The ionic hydrogels were synthesized using acrylamide (AAM) (Sinopharm Chemical Reagent Co., Ltd.) as monomers, *N,N*-methylenebisacrylamide (MBAA) (Sinopharm Chemical Reagent Co., Ltd.) as crosslinkers, 2-ketoglutaric acid (Shanghai Titan Scientific Co., Ltd.) as photoinitiators, and sodium chloride (NaCl) (Shanghai Macklin Biochemical Co., Ltd.) as ionic conductors. AAm powder (9.98 wt%) and NaCl (16.16 wt%) were dissolved in the deionized water. The concentration of prepared MBAA solution was 1.2 wt%. MBAA solution (1.13 wt%), 2-ketoglutaric acid (2.20 wt%) and AAm-NaCl solution (96.67 wt%) were mixed, followed by stirring for 30 min until they dissolved completely. The precursor solution was then poured into customized acrylic molds and cured by the ultraviolet light crosslinker (CL-1000L, Analytik Jena AG) with 365 nm wavelength (40 min).

Fabrication of Ultracapacitive Iontronic Pressure Sensors and Wearable Sensing Arrays: The ionic hydrogel was placed inside a spacer ring and sandwiched between two pieces of fabric electrodes. The conductive metal-plated fabrics (Shenzhen Changdasheng Electronics Co., Ltd.)

with a thickness of 100 μm were cut into desired shapes by using a laser cutting system (VLS3.50, Universal Laser Systems, Inc.), such as circular shapes of 3, 4, and 5 mm in radius for property tests. The spacer ring was made of silicone rubber (Ecoflex 00-30, Smooth-On Inc.). The Ecoflex precursor after vacuum degassing (15 min) was poured to pre-designed acrylic molds and then cured in an oven at 70 °C for 40 min. Finally, the assembled ultracapacitive iontronic pressure sensor was encapsulated using two VHB (4905, 3M) tapes. To fabricate sensing arrays, the material of spacer was substituted with polydimethylsiloxane (PDMS) owing to its larger elastic modulus. The matrix and curing agent of PDMS (Sylgard 184, Dow Corning Corp.) were mixed in a 10:1 weight ratio. The obtained PDMS precursor was degassed in a vacuum chamber for 15 min to remove air bubbles and then poured to pre-designed acrylic molds, followed by curing at 80 °C for 30 min. The 1D touch strip, 2D touch panel and shape recognition array were prepared with the same method as mentioned above except different layout patterns of pixels. The layouts and sizes of hydrogels, PDMS spacers, and conductive fabrics for wearable sensing arrays are shown in Figure S14 in the Supporting Information. It was further demonstrated that, with the 1 mm spacing between individual sensing pixels, there was limited signal crosstalk for the sensing functions of the multipixel arrays (Figure S15, Supporting Information).

Characterization and Measurements: To characterize the sensing performances of the sensors, a computer-controlled stepping motor-driven stage (HST-200, OptoSigma Inc.) equipped with a force gauge (LSB200, Futek Advanced Sensor Technology Inc.) was used to apply and measure the external pressure on the iontronic sensor. Meanwhile, the corresponding capacitance of the pressure sensor was accurately measured by using an LCR (inductance-capacitance-resistance) meter (E4980AL, Keysight Technologies Inc.). The unit area capacitance of the iontronic sensor was characterized referring to the common method.^[48] The test voltage across the sensors was measured by an oscilloscope (TBS 1102, Tektronix Inc.). The surface morphological features of the used conductive fabric electrode were obtained using atomic force microscopy (Dimension FastScan Bio AFM, Bruker Corp.) and scanning electron microscopy (JSM-7800F, JEOL Ltd.). The capacitance signals of wearable devices were real-time processed by using MATLAB (The MathWorks Inc.), and the operational results were displayed through a liquid crystal screen or an LED nixie tube. The soft bionic hand with the iontronic skin was attached to an industrial robot (Jaka Co., Ltd.). The input signal was transmitted to the industrial controller of the robot through TCP/IP (Transmission Control Protocol/Internet Protocol) via MATLAB. Linear sweep voltammetry of the ultracapacitive iontronic sensor was performed by using an electrochemical workstation (CS310, Wuhan Corrtest Instruments Corp., Ltd.) with a scan rate (10 mV s⁻¹).

Participant Recruitments: All experiments were conducted in accordance with the declaration of Helsinki and approved by the Institutional Review Board for Human Research Protections of Shanghai Jiao Tong University. The transradial amputees participated in this study were recommended by Shanghai Liankang Prosthetics and Orthotics Manufacturing Co., Ltd., Shanghai, China. The amputees were informed about the experimental procedure and signed the informed consent forms (ICFs) prior to the participation.

Supporting Information

Supporting Information is available from the Wiley Online Library or from the author.

Acknowledgements

This work was in part supported by the National Natural Science Foundation of China (Grant Nos. 52025057 and 91948302), the Science and Technology Commission of Shanghai Municipality (Grant No. 20550712100), and Shanghai Jiao Tong University Scientific and Technological Innovation Funds (2019QYB08).

Conflict of Interest

The authors declare no conflict of interest.

Author Contribution

G.G. and Z.S. conceived the idea and designed the study. Z.S. conducted the experiments. Z.S., G.G., C.M., and X.Z. analyzed and interpreted the results. G.G., C.M., and X.Z. directed the project. All the authors contributed to the writing and editing of the paper.

Data Availability Statement

The data that support the findings of this study are available from the corresponding author upon reasonable request.

Keywords

ionogel, pressure sensing, robotic skins, ultracapacitive, wearable electronics

Received: March 16, 2021

Revised: June 1, 2021

Published online:

- [1] X. Yu, Z. Xie, Y. Yu, J. Lee, A. Vazquez-Guardado, H. Luan, J. Ruban, X. Ning, A. Akhtar, D. Li, B. Ji, Y. Liu, R. Sun, J. Cao, Q. Huo, Y. Zhong, C. Lee, S. Kim, P. Gutruf, C. Zhang, Y. Xue, Q. Guo, A. Chempakasseril, P. Tian, W. Lu, J. Jeong, Y. Yu, J. Cornman, C. Tan, B. Kim, K. Lee, X. Feng, Y. Huang, J. A. Rogers, *Nature* **2019**, 575, 473.
- [2] S. Sundaram, P. Kellnhofer, Y. Li, J. Y. Zhu, A. Torralba, W. Matusik, *Nature* **2019**, 569, 698.
- [3] S. Lee, S. Franklin, F. A. Hassani, T. Yokota, M. O. G. Nayeem, Y. Wang, R. Leib, G. Cheng, D. W. Franklin, T. Someya, *Science* **2020**, 370, 966.
- [4] C.-C. Kim, H.-H. Lee, K. H. Oh, J.-Y. Sun, *Science* **2016**, 353, 682.
- [5] S. Y. Kim, Y. Choo, R. A. Bilodeau, M. C. Yuen, G. Kaufman, D. S. Shah, C. O. Osuji, R. Kramer-Bottiglio, *Sci. Rob.* **2020**, 5, eaay3604.
- [6] M. Amjadi, K.-U. Kyung, I. Park, M. Sitti, *Adv. Funct. Mater.* **2016**, 26, 1678.
- [7] C. Larson, B. Peele, S. Li, S. Robinson, M. Totaro, L. Beccai, B. Mazzolai, R. Shepherd, *Science* **2016**, 351, 1071.
- [8] L. E. Osborn, A. Dragomir, J. L. Betthausen, C. L. Hunt, H. H. Nguyen, R. R. Kaliki, N. V. Thakor, *Sci. Rob.* **2018**, 3, eaat3818.
- [9] T. G. Thuruthel, B. Shih, C. Laschi, M. T. Tolley, *Sci. Rob.* **2019**, 4, eaav1488.
- [10] J. A. George, D. T. Kluger, T. S. Davis, S. M. Wendelken, E. V. Okorokova, Q. He, C. C. Duncan, D. T. Hutchinson, Z. C. Thumser, D. T. Beckler, P. D. Marasco, S. J. Bensmaia, G. A. Clark, *Sci. Rob.* **2019**, 4, eaax2352.
- [11] J. W. Booth, D. Shah, J. C. Case, E. L. White, M. C. Yuen, O. Cyr-Choiniere, R. Kramer-Bottiglio, *Sci. Rob.* **2018**, 3, eaat1853.
- [12] T. Kim, S. Lee, T. Hong, G. Shin, T. Kim, Y.-L. Park, *Sci. Rob.* **2020**, 5, eabc6878.
- [13] J. A. Rogers, T. Someya, Y. Huang, *Science* **2010**, 327, 1603.
- [14] C. Majidi, *Soft Rob.* **2014**, 1, 5.
- [15] J. Y. Sun, C. Keplinger, G. M. Whitesides, Z. Suo, *Adv. Mater.* **2014**, 26, 7608.
- [16] C. M. Boutry, M. Negre, M. Jorda, O. Vardoulis, A. Chortos, O. Khatib, Z. Bao, *Sci. Rob.* **2018**, 3, eaau6914.

- [17] L. Pan, A. Chortos, G. Yu, Y. Wang, S. Isaacson, R. Allen, Y. Shi, R. Dauskardt, Z. Bao, *Nat. Commun.* **2014**, *5*, 3002.
- [18] G. Y. Bae, S. W. Pak, D. Kim, G. Lee, H. Kim do, Y. Chung, K. Cho, *Adv. Mater.* **2016**, *28*, 5300.
- [19] Z. Chen, Z. Wang, X. Li, Y. Lin, N. Luo, M. Long, N. Zhao, J. B. Xu, *ACS Nano* **2017**, *11*, 4507.
- [20] S. H. Park, H. B. Lee, S. M. Yeon, J. Park, N. K. Lee, *ACS Appl. Mater. Interfaces* **2016**, *8*, 24773.
- [21] X. Pu, M. Liu, X. Chen, J. Sun, C. Du, Y. Zhang, J. Zhai, W. Hu, Z. L. Wang, *Sci. Adv.* **2017**, *3*, e1700015.
- [22] H. Guo, X. Pu, J. Chen, Y. Meng, M.-H. Yeh, G. Liu, Q. Tang, B. Chen, D. Liu, S. Qi, C. Wu, C. Hu, J. Wang, Z. L. Wang, *Sci. Rob.* **2018**, *3*, eaat2516.
- [23] Z. Zhang, L. Wang, H. Yu, F. Zhang, L. Tang, Y. Feng, W. Feng, *ACS Appl. Mater. Interfaces* **2020**, *12*, 15657.
- [24] X. Y. Yin, Y. Zhang, J. Xiao, C. Moorlag, J. Yang, *Adv. Funct. Mater.* **2019**, *29*, 1904716.
- [25] B. Yang, W. Yuan, *ACS Appl. Mater. Interfaces* **2019**, *11*, 40620.
- [26] K. Meng, S. Zhao, Y. Zhou, Y. Wu, S. Zhang, Q. He, X. Wang, Z. Zhou, W. Fan, X. Tan, J. Yang, J. Chen, *Matter* **2020**, *2*, 896.
- [27] J. J. Lee, S. Gandla, B. Lim, S. Kang, S. Kim, S. Lee, S. Kim, *NPG Asia Mater.* **2020**, *12*, 65.
- [28] J. Lee, H. Kwon, J. Seo, S. Shin, J. H. Koo, C. Pang, S. Son, J. H. Kim, Y. H. Jang, D. E. Kim, T. Lee, *Adv. Mater.* **2015**, *27*, 2433.
- [29] V. Amoli, J. S. Kim, E. Jee, Y. S. Chung, S. Y. Kim, J. Koo, H. Choi, Y. Kim, D. H. Kim, *Nat. Commun.* **2019**, *10*, 4019.
- [30] N. Bai, L. Wang, Q. Wang, J. Deng, Y. Wang, P. Lu, J. Huang, G. Li, Y. Zhang, J. Yang, K. Xie, X. Zhao, C. F. Guo, *Nat. Commun.* **2020**, *11*, 209.
- [31] R. Li, Y. Si, Z. Zhu, Y. Guo, Y. Zhang, N. Pan, G. Sun, T. Pan, *Adv. Mater.* **2017**, *29*, 1700253.
- [32] X. Liu, J. Liu, S. Lin, X. Zhao, *Mater. Today* **2020**, *36*, 102.
- [33] Y. Huang, X. Fan, S. C. Chen, N. Zhao, *Adv. Funct. Mater.* **2019**, *29*, 1808509.
- [34] C. Yang, Z. Suo, *Nat. Rev. Mater.* **2018**, *3*, 125.
- [35] Y. Chang, L. Wang, R. Li, Z. Zhang, Q. Wang, J. Yang, C. F. Guo, T. Pan, *Adv. Mater.* **2020**, *33*, 2003464.
- [36] M. D. Bartlett, E. J. Markvicka, C. Majidi, *Adv. Funct. Mater.* **2016**, *26*, 8496.
- [37] Q. J. Sun, X. H. Zhao, Y. Zhou, C. C. Yeung, W. Wu, S. Venkatesh, Z. X. Xu, J. J. Wylie, W. J. Li, V. A. L. Roy, *Adv. Funct. Mater.* **2019**, *29*, 1808829.
- [38] R. S. Johansson, J. R. Flanagan, *Nat. Rev. Neurosci.* **2009**, *10*, 345.
- [39] K. O. Johnson, *Curr. Opin. Neurobiol.* **2001**, *11*, 455.
- [40] S. M. Maricich, S. A. Wellnitz, A. M. Nelson, D. R. Lesniak, G. J. Gerling, E. A. Lumpkin, H. Y. Zoghbi, *Science* **2009**, *324*, 1580.
- [41] W. W. Nichols, *Am. J. Hypertens.* **2005**, *18*, 3S.
- [42] G. Gu, N. Zhang, H. Xu, S. Lin, Y. Yu, G. Chai, L. Ge, H. Yang, Q. Shao, X. Sheng, X. Zhu, X. Zhao, *Nat. Biomed. Eng.* **2021**, unpublished.
- [43] F. Guan, Y. Xie, H. Wu, Y. Meng, Y. Shi, M. Gao, Z. Zhang, S. Chen, Y. Chen, H. Wang, Q. Pei, *ACS Nano* **2020**, *14*, 15428.
- [44] Y. Wang, H. Wu, L. Xu, H. Zhang, Y. Yang, Z. L. Wang, *Sci. Adv.* **2020**, *6*, eabb9083.
- [45] Y. Wu, Y. Liu, Y. Zhou, Q. Man, C. Hu, W. Asghar, F. Li, Z. Yu, J. Shang, G. Liu, *Sci. Rob.* **2018**, *3*, eaat0429.
- [46] C. Zhang, S. Liu, X. Huang, W. Guo, Y. Li, H. Wu, *Nano Energy* **2019**, *62*, 164.
- [47] G. Gu, H. Xu, S. Peng, L. Li, S. Chen, T. Lu, X. Guo, *Soft Rob.* **2019**, *6*, 368.
- [48] S. Li, N. Pan, Z. Zhu, R. Li, B. Li, J. Chu, G. Li, Y. Chang, T. Pan, *Adv. Funct. Mater.* **2019**, *29*, 1807343.